

Towards Laboratory Electron-Positron Plasma via Electromagnetic Showers in Matter

M. Pouyez,¹ G. Nicotera,² M. Galbiati,² T. Grismayer,³ L. Lancia,² C. Riconda,¹ and M. Grech²

¹*LULI, Sorbonne Université, CNRS, CEA, École Polytechnique,
Institut Polytechnique de Paris, F-75255 Paris, France*

²*LULI, CNRS, CEA, Sorbonne Université, École Polytechnique,
Institut Polytechnique de Paris, F-91128 Palaiseau, France*

³*GoLP/Instituto de Plasmas e Fusão Nuclear, Instituto Superior Técnico,
Universidade de Lisboa, 1049-001 Lisboa, Portugal*

The kinetic equations describing electromagnetic showers from high-energy electron beams interacting with targets are solved, building on the analytical framework developed in [Phys. Rev. Lett. **134**, 135001 (2025)]. Two regimes are defined by the ratio of the target thickness L to the radiation length L_r , which depends on the electron energy and target composition. For thin targets ($L < L_r$), we derive explicit expressions for the spectra of produced photons and pairs, as well as the number of pairs. For thick targets ($L > L_r$), we obtain the total pair number and photon spectrum. Analytical results agree well with Geant4 simulations, which show that significant pair escape requires $L < L_r$. The divergence, density and characteristic dimensions of the escaping pair jets are obtained, and a criterion for pair plasma formation is derived. While current laser wakefield beams are not well adapted, multi-petawatt lasers may provide new electron or photon sources suitable for laboratory pair plasma production, opening new avenues for studying extreme plasma astrophysics in the laboratory.

I. INTRODUCTION

When a high-energy electron or positron interacts with the intense electric field of a nucleus, it has a probability to radiate its energy via the Bremsstrahlung process. The emitted photon, also interacting with the nucleus field [1], can in turn transform into an electron-positron pair via the Bethe-Heitler process [1]. This interplay of photon emission and pair creation initiates a cascade of secondary particles, also known as an electromagnetic shower (EMS).

EMS in matter are extensively studied in particle physics as well as astrophysics [2–5]. With the emergence of ultra-high intensity lasers, and even more so since the advent of petawatt-class laser systems [6–14] capable of producing high-energy electron [15–22] and photon [23–31] beams together with extremely intense electromagnetic (EM) fields, EMS have also gained the attention of the laser-plasma community [32–42]. While these later works focused on EMS developing in strong EM fields rather than matter, EMS in matter are still considered a promising path toward the generation of quasi-neutral electron-positron pair plasmas in the laboratory [43–50]. Producing such plasmas would unlock the experimental investigation of various processes - from plasma instabilities to particle acceleration - of utmost importance for extreme plasma astrophysics [51–53].

The theoretical study of EMS in matter began in the 1930's, motivated by the then recent discovery of cosmic ray showers [54]. The mathematical description of such showers was developed almost simultaneously by Bhabha and Heitler [55] and by Carlson and Oppenheimer [56] in 1937. Further descriptions were established at the beginning of the 1940's [57–59] and today, the book of Rossi and Greisen [60] remains one of the most detailed and clear mathematical analyses of the EMS evolution.

The angular structure of the EMS was first addressed by Molière [61], who provided a key estimate for the angular spread of shower particles at a given thickness. Further analytical analyses [62–67] have extended this work by solving the full three-dimensional diffusion equation for different shower depths (length traversed by the primary particle).

However, all these advanced analytical tools rely on several approximations for the shower depth, particle energies and rate definitions. As a result, they fall short of providing an analytical framework for describing the production of an electron-positron pair plasma from the collision of an electron beam with matter. In particular, a good way to estimate the density of the jet of pairs emerging from such a collision is yet to be found.

In this work, we address this problem. To do so, we rely on the analytical framework developed in [68] to describe EMS developing in strong EM fields, which we adapt to EMS in matter. This allows us to derive explicit expressions for the number of pairs produced per incident particle (N_{\pm}/N_0), henceforth referred to as the shower multiplicity, as well as for the produced pair and photon spectra. These expressions are thoroughly benchmarked against Monte-Carlo simulations, and in particular Geant4 simulations. Additionally, these simulations allow us to characterize the divergence of the pairs escaping the target. Together, these studies provide us with simple estimates for the characteristic density and size of the pair jets emerging from the target, and thus allow us to identify the conditions under which a pair plasma could be produced.

Throughout the paper, we used SI units and standard notations for physical constants: c denotes the speed of light in vacuum, m the electron mass, e the elementary charge, ϵ_0 the permittivity of vacuum and \hbar the reduced Planck constant. The fine structure constant is denoted

by $\alpha = e^2/(4\pi\epsilon_0\hbar c)$, and $r_e = e^2/(4\pi\epsilon_0 m_e c^2)$ denotes the classical radius of the electron.

II. NUMBER OF PAIRS

In this section, we aim to determine the number of pairs generated by an initial population of electrons with energy $\gamma_0 mc^2$ as it interacts with a mono-atomic target.

Our starting point is the cascade equations written for successive generation of leptons and photons [40]: a lepton of generation n creates photons of generation n , which in turn produce new pairs of generation $n+1$. The temporal evolution of the energy distributions of each generation (n) of electrons ($-$), positrons ($+$), and photons (γ) read¹:

$$\begin{aligned} \partial_t f_{\pm}^{(n)}(\gamma, t) &= \int_0^\infty d\gamma_\gamma w(\gamma + \gamma_\gamma, \gamma_\gamma) f_{\pm}^{(n)}(\gamma + \gamma_\gamma, t) \\ &\quad - W(\gamma) f_{\pm}^{(n)}(\gamma, t) \\ &\quad + \int_0^\infty d\gamma_\gamma \bar{w}(\gamma_\gamma, \gamma) f_{\gamma}^{(n-1)}(\gamma_\gamma, t), \end{aligned} \quad (1)$$

$$\begin{aligned} \partial_t f_{\gamma}^{(n)}(\gamma, t) &= \int_1^\infty d\gamma w(\gamma, \gamma_\gamma) f_{-}^{(n)}(\gamma, t) \\ &\quad + \int_1^\infty d\gamma w(\gamma, \gamma_\gamma) f_{+}^{(n)}(\gamma, t) \\ &\quad - \bar{W}(\gamma) f_{\gamma}^{(n)}(\gamma, t), \end{aligned} \quad (2)$$

where $(\gamma - 1)mc^2$ is the lepton kinetic energy, $\gamma_\gamma mc^2$ is the photon energy, and $w(\gamma, \gamma_\gamma)$ and $\bar{w}(\gamma_\gamma, \gamma)$ are the energy differential rates of photon emission (Bremsstrahlung process) and pair production (Bethe-Heitler process), respectively. We have also introduced $W(\gamma) = \int_0^\infty d\gamma_\gamma w(\gamma, \gamma_\gamma)$ and $\bar{W}(\gamma) = \int_1^\infty d\gamma_\gamma \bar{w}(\gamma_\gamma, \gamma)$.

Multiple definitions of the Bremsstrahlung and Bethe-Heitler cross-sections exist in the literature [69, 70]. In this work, we adopt the formulations used in [71] and the corresponding differential rates w and \bar{w} are recalled in the *Supplemental Material* [72]. These rates are different from the ones used in Geant4, that rely on interpolated data from Seltzer and Berger [73, 74]. As will be shown later in this work, this difference does not impact the overall study as it mainly leads to a systematic overestimate (by a factor ~ 1.5) of the total Bremsstrahlung cross-section. Furthermore, using the cross-sections from [71] rather than the Seltzer and Berger data [73, 74] has two advantages: it provides us with an analytical model for the cross-sections, and it can be applied to both neutral and ionized targets.

A. Radiation time

To solve the kinetic Eqs. (1) and (2), we follow the methodology developed in [68] and introduce the radiation time T_r (equivalently radiation length $L_r = cT_r$):

$$T_r = \int_1^{\gamma_0} \frac{d\gamma}{\int_0^\infty d\gamma_\gamma \gamma_\gamma w(\gamma, \gamma_\gamma)} \quad (3)$$

$$\xrightarrow{\gamma_0 \gg 1} \frac{\ln(\gamma_0)}{K(n_i, Z, Z^*, T)} \quad (4)$$

where K , which has the dimension of a frequency, is a function of the target atomic density n_i , atomic number Z , ionization degree Z^* , and temperature T . Its full expression is provided in the *Supplemental Material* [72]. In the following, we restrict our study to neutral targets, and K is a function of n_i and Z only:

$$K(n_i, Z) = 4 Z^2 n_i r_e^2 c \alpha \left[\frac{4}{3} I(0) + \frac{13}{9} - \frac{4}{3} f_C(Z) \right] \quad (5)$$

with $I(0) = \frac{1}{2} \left[\ln \left(1 + \bar{L}_{\text{TF}}^2 \right) - \bar{L}_{\text{TF}}^2 / (1 + \bar{L}_{\text{TF}}^2) \right]$ a function of the Thomas-Fermi length normalized to the Compton radius $\bar{L}_{\text{TF}} = Z^{-1/3} \alpha^{-1}$, and f_C the Coulomb correction defined as:

$$f_C(Z) = \frac{\alpha^2 Z^2}{1 + \alpha^2 Z^2} \sum_{n=1}^{\infty} (-\alpha^2 Z^2)^n [\zeta(2n+1) - 1]. \quad (6)$$

In this framework, the radiation time refers to the time over which an electron loses all of its kinetic energy through Bremsstrahlung radiation. This differs from the radiation time commonly used in the literature, which corresponds to the time over which an electron reduces its energy by a factor $1/e$ through radiation. However, with that definition, an electron continues to contribute to the shower development after the radiation time. In contrast, with the definition Eq. (4), the radiation time delimits the moment where the electron ceases to participate to the photoemission.

In the following, it is also convenient to express distance in units of radiation length $L_r = cT_r$. We have reported in Fig. 1 the value of $L_r / \ln(\gamma_0) = c/K(n_i, Z)$ for different relevant elements of the periodic table in a neutral state and at standard conditions of temperature and pressure.

B. Short-time solution

At a time $t \ll T_r$, the incident electrons have not yet cooled down, and we can neglect the radiative operator in the leptons dynamics [first two terms of Eq. (1)]. Furthermore, $\forall \gamma_\gamma \bar{W}(\gamma_\gamma) t \ll 1$ we Taylor expand² the pho-

¹ Under the approximation that all particles propagate at the speed of light

² Using the asymptotic definition of the rates, this approximation breaks down for $t/T_r \gtrsim 2/\ln(\gamma_0 - 1)$. Nevertheless, this approximation still holds for a wide range of times and energies (Example: for $\gamma_0 = 10^5$, it is a good approximation until $t/T_r \lesssim 1/6$)

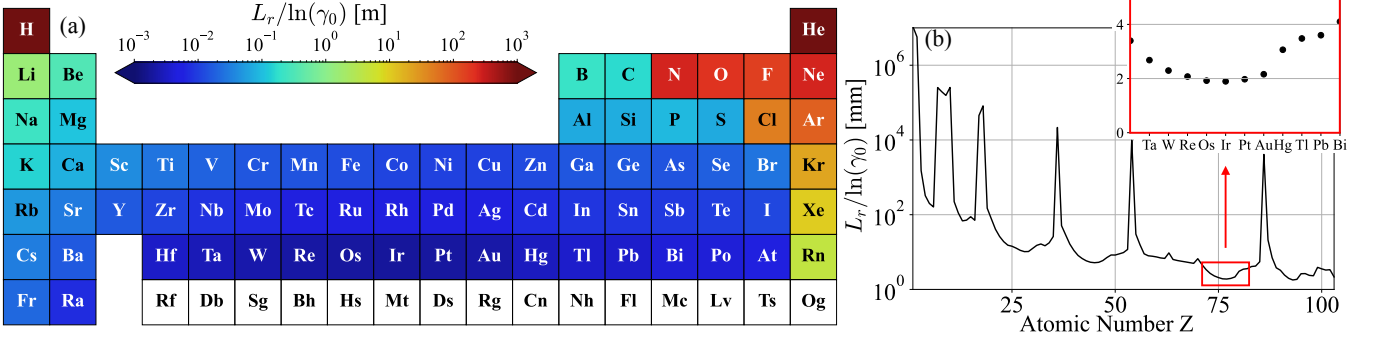


FIG. 1. Radiation length L_r normalized to $\ln(\gamma_0)$ for relevant elements of the periodic table in a neutral state and at standard conditions of temperature and pressure (a) and as a function of the atomic number (b).

ton pair creation probability $1 - \exp[-\bar{W}(\gamma_\gamma)t]$. Solving the kinetic Eqs. (1) and (2) under these two assumptions, we obtain:

$$f_\gamma^{(n-1)}(\gamma_\gamma, t) \simeq \frac{2^{n-1}}{(2n-1)!} G^{(n-1)}(\gamma_\gamma) \left(\frac{t}{T_r}\right)^{2n-1}, \quad (7)$$

$$f_\pm^{(n)}(\gamma, t) \simeq \frac{2^{n-1}}{(2n)!} L^{(n)}(\gamma) \left(\frac{t}{T_r}\right)^{2n}, \quad (8)$$

with

$$G^{(n)}(\gamma_\gamma) = \int_1^\infty d\gamma T_r w(\gamma, \gamma_\gamma) L^{(n)}(\gamma), \quad (9)$$

$$L^{(n)}(\gamma) = \int_0^\infty d\gamma_\gamma T_r \bar{w}(\gamma_\gamma, \gamma) G^{(n-1)}(\gamma_\gamma), \quad (10)$$

$$L^{(0)}(\gamma) = f_-^{(0)}(\gamma, t=0). \quad (11)$$

We find that the spectrum of the n th generation of pairs grows as $(t/T_r)^{2n}$. In the limit $t \ll T_r$, the first generation thus dominates the total pairs. Therefore, the integration of $f_\pm^{(1)}$ over energy leads to a good estimate for the number of produced pairs. For N_0 incident electrons at $\gamma_0 mc^2$, the shower multiplicity N_\pm/N_0 reads:

$$N_\pm(t)/N_0 = \left(\frac{t}{T_r}\right)^2 \frac{T_r^2}{2} \int_0^{\gamma_0-1} d\gamma_\gamma \bar{W}(\gamma_\gamma) w(\gamma_0, \gamma_\gamma) \xrightarrow{\gamma_0 \gg 1} \frac{1}{2} \left(\frac{t}{T_r}\right)^2 \frac{R(n_i, Z)}{K(n_i, Z)} \ln(\gamma_0)^2 \ln(c_1 \gamma_0). \quad (12)$$

where $c_1 = 0.016$ and where the functions R and K are given in [72]. Interestingly, the only dependence on the target properties is contained in the ratio R/K and the radiation time. For a non-ionized material, the ratio R/K is a function of the atomic number Z only and decreases very slowly: from 0.570 to 0.568 for $Z \in [10, 100]$.

C. Long-time solution

The number of pairs can also be derived in the long-time-scale regime using the methodology presented in

[68]. The proper mathematical derivation is provided in the Supplementary Material [72], here, we outline the main approximations of the calculation.

The first assumption is that all leptons have already radiated their energy into photons. By computing the total photon spectrum emitted by a single lepton, we establish a relation between the spectrum of all emitted photons of generation n and the spectrum of the pairs of generation n at the moment of their creation.

Second, we assume that over such a time scale, the probability of the pair production process is close to a Heaviside function evaluated in $\gamma_\gamma - \gamma_c$, where γ_γ is the energy of the parent photon and γ_c is a threshold energy. This assumption means that only the photons created with an energy larger than γ_c have produced pairs. The critical energy γ_c is chosen as the photon energy below which other processes dominate over pair production. It was extracted from the NIST database [75] as the energy for which the photon scattering rate becomes equal to the pair production rate. For neutral materials, a fit provides:

$$\gamma_c(Z) = \frac{237.6}{Z} + \frac{27.5}{Z^{1/3}}. \quad (13)$$

Finally, we assume that, upon pair production, a photon transfers half of its energy to each resulting lepton.

The first approximation provides us with the total photon spectrum emitted by a given population of leptons. The second approximation identifies the photons that participate in the pair production, and the third approximation defines how these photons split their energy into the new pairs. Using these approximations, we obtain a recursive relation between the number of pairs $N_\pm^{(n)}$ and the total photon spectrum $F_\gamma^{(n)}$ of generation (n) . For $n \leq \ln(\gamma_0/\gamma_c)/\ln(2)$ the total photon spectrum is:

$$F_\gamma^{(n)}(\gamma_\gamma) = \frac{2^n}{(2n+1)!} \frac{1}{\gamma_\gamma} \ln\left(\frac{\gamma_0}{2^n \gamma_\gamma}\right)^{2n+1} \Theta(\gamma_0 - 2^n \gamma_\gamma) \quad (14)$$

while the number of pairs of generation (n) reads:

$$N_{\pm}^{(n)}/N_0 = \frac{2^{n-1}}{(2n)!} \ln \left(\frac{\gamma_0}{2^{n-1}\gamma_c} \right)^{2n} \Theta(\gamma_0 - 2^{n-1}\gamma_c). \quad (15)$$

From the Heaviside function Θ in equation (15) we obtain that the maximal number of generations is given by $n = \ln(\gamma_0/\gamma_c)/\ln(2) + 1$. Furthermore, the final number of pairs is obtained by summing this equation over all generations. In the limit $\gamma_0 \rightarrow \infty$, taking the continuous limit for the sum and using a saddle-point approximation for the integral, we finally obtain:

$$N_{\pm}/N_0 = \frac{1}{2 + \ln(2)} \frac{\gamma_0}{\gamma_c(Z)} \quad (16)$$

where the only material dependence is now contained in the photon threshold energy $\gamma_c(Z)$.

D. Comparison with simulations

In this section, we compare analytical predictions of pair production with numerical results obtained from both Geant4 simulations and numerical integration of Eqs. (1) and (2). The numerical integration is carried out using an in-house Monte Carlo (MC) code that includes only Bremsstrahlung and Bethe–Heitler processes, with cross-sections defined in [71]. We refer to these results as MC simulations throughout the text. In contrast, the Geant4 simulations incorporate broader physical processes: for photons, the pair production, the Compton scattering, and the photoelectric processes, while for leptons, the Bremsstrahlung, the ionization, the multiple Coulomb scattering, and the annihilation processes.

In Figure 2 we present the total number of produced pairs by the collision of electrons with a neutral target of tantalum under standard temperature and pressure conditions. Panel (a) represents the number of pairs as a function of the target thickness L/L_r for 10 GeV incident electrons, while panels (b) and (c) show the dependence on incident electron energy γ_0 for thin ($L/L_r = 10^{-2}$) and thick ($L/L_r = 10^2$) target respectively.

The number of pairs derived for short-time Eq. (12) and long-time Eq. (16) interaction are represented in solids black lines (where we use the relation $L/L_r = t/T_r$). The total number of pairs calculated using Geant4 simulations is shown as green circles, while the number of pairs collected on a detector right after the target is presented in green dots. The solutions of the EMS using the MC simulations are shown as a red line in panel (a), and as red dots in panels (b) and (c). The maximum number of pairs predicted by Eq. (16), using a threshold value of $\gamma_c = 2$ (natural threshold for Bethe-Heitler process) is indicated by the black dashed line.

Excellent agreement between theory, Geant4 simulations and numerical solutions of Eqs. (1) and (2) are found in both asymptotic regimes. In the case of a thin target, the slight discrepancy between the Geant4 results

and the theoretical or MC simulations arises from the differences in the cross-section definitions. The decrease in the number of outgoing pairs (green dots) beyond the radiation length indicates that leptons get trapped within the material. Indeed, after traveling a distance $L \sim L_r$ through the target, most of the leptons have cooled down and processes such as ionization and collisions become dominant, that confine the pairs inside the material. As a results, to maximize the number of outgoing pairs and, consequently, the plasma density, it is optimal to use a target with a thickness smaller than L_r . For such small target thickness, an excellent agreement between Geant4 simulations and Eq. (12) is found. Similarly, a very good agreement between Geant4 results and Eq. (16) is found for thick targets. Although this particular solution has no practical importance for pair plasma production, it is a fundamental aspect of the shower development, as well as important to determine the total energy deposition, e.g. in calorimeters for particle physics [2].

Finally, we note that, although Fig. 2 focuses on a Tantalum target, the short-time predictions are universal across different target materials, as long as the ratio L/L_r is similar. In contrast, the long-time regime becomes material-dependent through the critical energy γ_c .

Let us now turn to Fig. 3 that provides the spectrum of electron-positron pairs (a) and photons emerging (b) from the collision of 10 GeV electrons with a Tantalum target of thickness $L = 10^{-2}L_r$ and $L = 10^2L_r$, respectively. In Fig. 3(a), the analytical pair spectrum given by Eq. (8) considering only $n = 1$ (in black) is compared to Geant4 (in blue) and MC (in red) simulations and are found in excellent agreement. The slight differences are explained by the discrepancies on the cross-section as mentioned before. Figure 3 (b) shows the spectrum of all generated photons during the interaction with a thick target. The solid black curve, computed by summing over all generations Eq. (14) and the blue curve, obtained from Geant4 simulations³ correspond to the total photon spectrum emitted during the interaction. The red curve represents the Geant4 spectrum of photons that have generated a pair, while the vertical black dashed line indicates the threshold energy γ_c . Our analysis predicted a sharp threshold in the photon spectrum responsible for pair production near γ_c . However, because the photon scattering probability does not behave like a Heaviside step function at γ_c , this sharp cutoff does not appear in the Geant4 simulations. Nevertheless, by slightly overestimating the contributions from photons just above γ_c and neglecting those just below it, integrating the total photon spectrum from γ_c to infinity still yields to an accurate estimate of the number of pairs as demonstrated by Fig. 2.

³ MC simulation results are not included here, as they do not account for all significant processes in this regime.

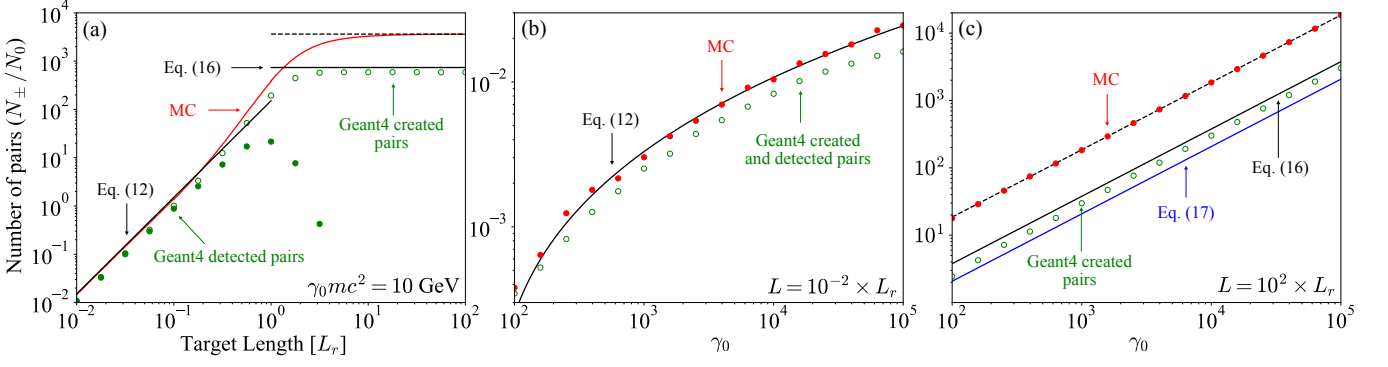


FIG. 2. Number of produced pairs in the collision of electrons with Tantalum $Z = 73$. In panel (a) as a function of the target thickness L for 10 GeV incident electrons. In panels (b) and (c) as a function of the incident electron energy γ_0 for $L/L_r = 10^{-2}$ and $L/L_r = 10^2$, respectively. The black curves represent the solutions from this work, given by Eqs. (12) and (16), while the blue line corresponds to Heitler's model, Eq. (17). Dashed black lines indicates the solution of Eq.(16) with $\gamma_c = 2$. The red line in panel (a) and red dots in panels (b) and (c) show the results from the MC simulations. Green circles denote the total number of pairs and green dots represent the number of outgoing pairs extracted from Geant4 simulations.

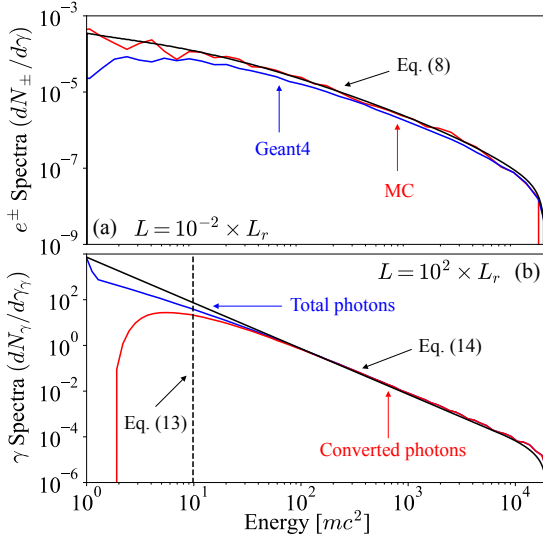


FIG. 3. Spectra of (a) electron-positron pairs and (b) photons resulting from the collision of 10 GeV electrons with a Tantalum target of thickness $L = 10^{-2}L_r$ and $L = 10^2L_r$ respectively. In panel (a), the black line stands for Eq. (8) ($n=1$), while the blue and red curves are obtained from Geant4 and MC simulations, respectively. In panel (b), the black line represents the total photon spectrum obtained by summing Eq. (14) over each generation, and the black dotted line corresponds to Eq. (13). The blue and red curve, extracted from Geant4 simulations, represents, respectively, the total photon spectrum and the spectrum of all the photons that have generated pairs.

E. Comparison with previous solutions

1. Solutions with Mellin transform

In 1938, Landau and Rumer [57] solved the diffusion equations, or equivalently the kinetics equations,

by applying the Mellin transform with respect to energy for the distribution functions. By considering the rates of Bremsstrahlung and Bethe-Heitler processes in the asymptotic limit $1 \ll \gamma, \gamma_\gamma \ll \gamma_0$, they compute the distribution of pairs and photons in Mellin space. The solution takes the form of a sum of two exponential terms, one of which they neglect to compute the inverse Mellin transform. This last approximation is only valid for a time not too small [60], meaning their solution can not accurately describe the system at very short time scale.

Moreover, since the number of pairs is $N_\pm(t) = \int_1^{\gamma_0} d\gamma f_\pm(\gamma, t)$ and the pair spectrum is derived in the limit $\gamma \gg 1$, the total number of pairs can not be obtained. However, the number of pairs with an energy greater than some threshold γ is well represented by $\int_\gamma^{\gamma_0} d\gamma' f_\pm(\gamma', t)$ in the limit $1 \ll \gamma \ll \gamma_0$. For the long-time scale regime, the leptons have already cooled down and their energy approaches mc^2 . It follows that their solution no longer captures the pair population in the long-time scale regime.

Thus, all the solutions and their approximate form obtained in this framework [57–60, 66] are representative of the EMS evolution only in the intermediate time regime $t \sim T_r$, while our solutions complete the description for the asymptotic regimes $t \ll T_r$ and $t \gg T_r$.

2. Heitler's model

One of the simplest and most useful tools for the description of EMS is the toy model introduced by Heitler [76]. It is now commonly used in a large physics community to estimate the final number of pairs emerging from EMS: in astrophysics for magnetic showers [77], in high-energy particle physics for hadronic shower [78] and in the strong-field community where a generalization to arbitrary splitting ratios has been proposed recently [79]. In this heuristic model, the electron (or positron) radiates

a photon after travelling a length $d = \ln(2)c/W$, where d corresponds to the length for which a lepton loses half of its energy through radiation. Similarly, after travelling d , the photon generates a pair, giving half of its energy to each of the outgoing leptons. These processes stop when leptons reach a critical energy noted \mathcal{E}_c . Heitler shows that the final number of pairs then reads⁴:

$$N_{\pm}/N_0 = \frac{\gamma_0 mc^2}{3\mathcal{E}_c}. \quad (17)$$

This asymptotic solution closely aligns with the one obtained in this work, Eq. (16). Both exhibit the same energy dependence, $N_{\pm} \propto \gamma_0$, but they differ in their essence and in the definition of the critical energy. In this work, we prove that if only the two QED channels are considered, i.e. Bremsstrahlung and Bethe-Heitler, the factor in front of γ_0/γ_c should tend towards $(2+\ln(2))^{-1} \simeq 0.37$ when $\gamma_0 \rightarrow \infty$. By contrast, Heitler's model yields a slightly lower prefactor of $1/3$. However, by choosing a heuristic rate, the photon emitted always receives the same fraction of the lepton energy, and low-energy photons can be emitted only by low-energy leptons. In our framework, low-energy photons are continuously emitted and follow the full Bremsstrahlung spectrum. Furthermore, Heitler defines the critical energy using a condition on the electron processes, while we use a condition on the photon instead. The critical energy of the Heitler model is indeed defined as the value for which the energy lost by radiation is of the same order of magnitude as the energy lost by ionization. It reads [2, 76]:

$$\mathcal{E}_c(Z)/mc^2 = \frac{1193.7}{Z + 1.24}, \quad (18)$$

while the critical energy of this work [Eq. (13)] corresponds to the value for which the photon scattering rate equals the pair production rate. Overall, these differences lead to a factor ~ 2 between our model and the one of Heitler [76] for the maximal number of produced pairs.

III. DIVERGENCE OF PRODUCED PAIRS

An analytical expression for the number of electron-positron pairs produced during short and long interactions has been established, we now turn to the divergence angle of the outgoing pairs.

As outlined in the introduction, several advanced analytical studies on the angular distribution of shower particles were conducted in the 1950s [61–67]. By solving the three-dimensional diffusion equation for EMS considering the angular differential cross section for Bremsstrahlung, Bethe-Heitler, Ionization and multiple Coulomb scattering processes, they were able to estimate the radial distribution of the outgoing pairs. The Kamata and Nishimura model [67] remains the most widely adopted, offering a simple and practical approximation for the radial distribution of shower particles.

However, this solution relies on several simplifying assumptions that lead to notable inaccuracies, as confirmed by later numerical studies [80, 81]. These limitations are thoroughly reviewed in [82] and were partially addressed in Sec. II E.

Furthermore, one of the main contributions to the angular spread of the outgoing pairs is the Multiple Coulomb Scattering (MCS) angles which has already been studied in [60, 83–87]. In these works, authors have estimated the root mean square (RMS) angle resulting from MCS only. Under the assumption of a Gaussian angular distribution, Rossi and Greisen [60] have shown that the RMS angle scales as $\propto \gamma_0^{-1}\sqrt{L}$, and demonstrated that when L is expressed in units of radiation length, it becomes independent of the material. However, the accumulation of MCS contributes to a large tail in the angular distribution function [87], making the Gaussian approximation unreliable and the RMS angle a poor descriptor of the angular spread.

As a result, these models fail to provide a reliable estimate of the divergence angle of the outgoing pairs. As emphasized by Capdevielle and Gawin [88], only Monte Carlo simulations can accurately reproduce the radial profile of shower particles in our regime of interest. Nonetheless, the scaling laws derived from these previous studies will guide our upcoming parametric analysis.

We performed $16 \times 16 \times 17$ Geant4 simulations⁵ for 16 different atomic numbers (ranging from 6 to 82), 16 different incident energy (logarithmically spaced from 100 MeV to 50 GeV) and 17 different target lengths (logarithmically spaced from $L/L_r = 10^{-3}$ to $L/L_r = 10$)⁶. For each simulation, we recorded p_{\perp} and p_{\parallel} , the perpendicular and parallel components to the incident electrons direction of the outgoing positrons. We choose to characterize only the properties of the positrons to exclude the contribution from the incident electrons. This approach is equivalent to characterizing the properties of the resulting pairs, as the electrons and positrons produced in the interaction are generated symmetrically. From this, we reconstruct the angular distribution of the outgoing pairs $dN_{\pm}/d\theta$ where $\theta = \arctan(p_{\perp}/p_{\parallel})$.

⁴ In the second edition of his book [76] page 234, Heitler introduces a supplementary factor $1/3$ to take the critical energy into account correctly. He corrected this in the third edition, page 388, introducing instead a factor $1/\kappa$, with κ of order unity. In this work, we use the formula given in the third edition with $\kappa = 1$ and divided by 2 to account only for the number of pairs and not for the total number of leptons as he did.

⁵ The physic's list used here is the same as the one defined in Sec. II D.

⁶ We focus exclusively on the short interaction regime as it is the relevant regime for plasma production, as discussed in Sec. II D.

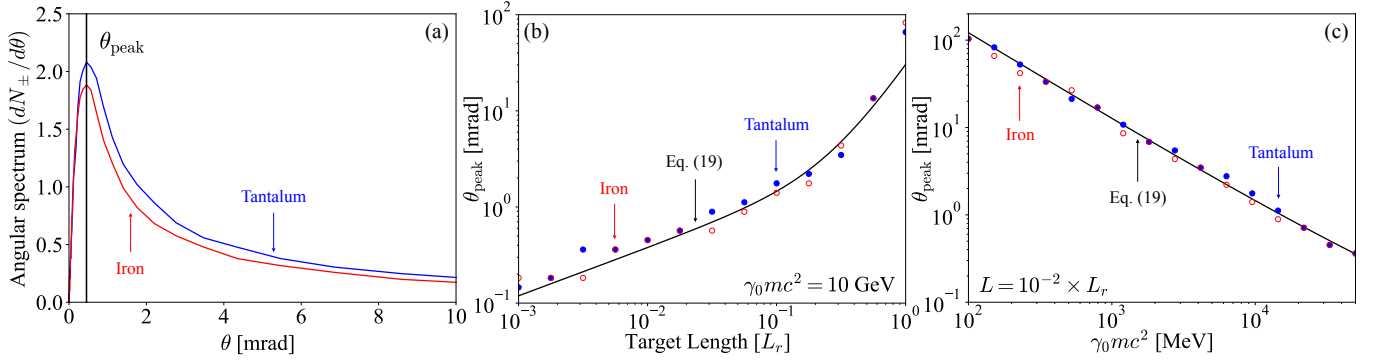


FIG. 4. In panel (a), the angular distribution of the outgoing pairs $dN_{\pm}/d\theta$ for 10 GeV incident electrons colliding with a target of length $L = 10^{-2}L_r$. In panels (b) and (c) the angle θ_{peak} as a function of the target length (for 10 GeV incident electron) and as a function of initial electron energy (for $L = 10^{-2}L_r$). Results for Tantalum and Iron converters are shown in red and blue. The black curve stands for Eq. (19).

In Fig. 4(a), we present the angular distribution $dN_{\pm}/d\theta$ of the outgoing pairs resulting from the collision of 10 GeV electrons with Tantalum (red) and Iron (blue) targets of length $L = 10^{-2}L_r$. We find that the angle at which the distribution $dN_{\pm}/d\theta$ is maximized, denoted θ_{peak} , is given by:

$$\theta_{\text{peak}}(\gamma_0, L) = \frac{c_2}{\gamma_0} \sqrt{\frac{L}{L_r}} + \frac{c_3}{\sqrt{\gamma_0}} \left(\frac{L}{L_r} \right)^2 \quad (19)$$

where $c_2 \simeq 73.6$ and $c_3 \simeq 3.7$ are fitting parameters. The position of θ_{peak} for both materials is also displayed with a black straight line. For short interactions, similar dependencies as the ones discussed in [60, 83, 86, 87] for the RMS MCS angle are found: θ_{peak} grows with $\sqrt{L/L_r}$, decrease as γ_0^{-1} and is independent of the material when L is expressed in unit of the radiation length.

To highlight the different dependencies and assess the validity of the fit, we also show in panels (b) and (c) the angle θ_{peak} as a function of the target length (for 10 GeV incident electron) and as a function of initial electron energy (for $L = 10^{-2}L_r$) in the cases of Tantalum (red) and Iron (blue) converters. As depicted in this figure, the fitted function given by Eq. (19) accurately describes θ_{peak} for $L < L_r$, which is the regime of interest for pair plasma production.

Here, we chose to focus solely on θ_{peak} because as it will be shown in the next section, it provides a reliable estimate for the outgoing pair density.

IV. TOWARD PAIR PLASMA IN THE LABORATORY

Having determined both the number of electron-positron pairs and their divergence angle as functions of the incident electron energy and target parameters, we are now able to estimate the pair density. This estimation ultimately yields a straightforward criterion on

initial source and target parameters for the achievement of the plasma state.

To obtain a pair plasma, the outgoing beam should first satisfy the quasi-neutrality $N_+ \sim N_-$, and secondly, to ensure collective behaviour, its size should exceed the skin depth δ [49]:

$$\delta = \sqrt{\frac{\varepsilon_0 mc^2 \langle \gamma_{\pm} \rangle}{2e^2 n_{\pm}}} \quad (20)$$

where n_{\pm} is the pairs density and $\langle \gamma_{\pm} \rangle$ is the average energy of the outgoing pairs.

In this section, we estimate and optimize the pair beam density to finally discuss the plasma feasibility.

A. Outgoing pair density

We adopt polar coordinates defining $(x_{\perp}, x_{\parallel})$ as the transverse and longitudinal positions of the positrons (or equivalently of the generated electrons). We introduce the spatial angle $\theta_x = \arctan(x_{\perp}/x_{\parallel})$ to describe their trajectory. Assuming the positrons are ultra-relativistic with $v_{\perp} \ll v_{\parallel} \simeq c$ and $\theta_{\text{peak}} \ll 1$, we have $dx_{\parallel}/dt = c$ and $dx_{\perp}/dt \simeq c\theta_{\text{peak}}$. Integrating the equation of motion, we obtain for $x_{\parallel} \leq L$:

$$x_{\perp} = x_{\parallel} \left[\frac{2}{3} \frac{c_2}{\gamma_0} \sqrt{\frac{x_{\parallel}}{L_r}} + \frac{1}{3} \frac{c_3}{\sqrt{\gamma_0}} \left(\frac{x_{\parallel}}{L_r} \right)^2 \right], \quad (21)$$

and for $x_{\parallel} \geq L$,

$$x_{\perp} = x_{\parallel} \left[\frac{c_2}{\gamma_0} \sqrt{\frac{L}{L_r}} \left(1 - \frac{1}{3} \frac{L}{x_{\parallel}} \right) + \frac{c_3}{\sqrt{\gamma_0}} \left(\frac{L}{L_r} \right)^2 \left(1 - \frac{2}{3} \frac{L}{x_{\parallel}} \right) \right]. \quad (22)$$

We model the incoming N_0 electrons as a cylindrical bunch of length L_b and radius R_b . We neglect the ini-

tial divergence of the beam as the dominant contribution arises from interactions within the target⁷. Since all the particles are assumed to travel at a velocity $v_{\parallel} \simeq c$, the longitudinal size of the emerging pair beam remains approximately L_b immediately after exiting the target.⁸ Considering the electron-positron beam as a cylinder, the radius of the beam is estimated as $R_{\pm} \simeq R_b + x_{\perp}$ and the plasma density finally reads $n_{\pm} \simeq N_{\pm}/(\pi L_b R_{\pm}^2)$. Just after the target, we have:

$$n_{\pm} = \frac{c_4 N_0 (L/L_r)^2 \ln(\gamma_0)^2 \ln(c_1 \gamma_0)}{2\pi L_b [R_b + L_r g(\gamma_0, L/L_r)]^2} \quad (23)$$

where $c_4 = R(n_i, Z)/K(n_i, Z) \simeq 0.569$ for a neutral target and

$$g(\gamma_0, L/L_r) = \frac{2}{3} \frac{c_2}{\gamma_0} \left(\frac{L}{L_r} \right)^{3/2} + \frac{1}{3} \frac{c_3}{\sqrt{\gamma_0}} \left(\frac{L}{L_r} \right)^3. \quad (24)$$

The optimization of the pair density is now studied to predict the maximal density reachable in the laboratory.

Equation (23) shows that the pair density depends independently on the radiation length L_r and the normalized target thickness L/L_r . Since L_r is material-specific, the density is inherently dependent on the target composition. For a fixed target length, the density always decreases with increasing L_r , emphasizing that minimizing the radiation length is key to optimizing plasma density. As shown in the insert of Fig. 1(b), the optimal material is Iridium ($Z = 77$) and its neighbours (Osmium and Platinum) with a radiation length of $L_r = 1.89 \ln(\gamma_0)$ mm. For comparison with commonly used materials [48, 50], Lead ($Z = 82$) and Tantalum ($Z = 73$) have a radiation length of $L_r = 3.60 \ln(\gamma_0)$ mm and $L_r = 2.68 \ln(\gamma_0)$ mm respectively. As a result, the maximum density achievable with Lead or Tantalum is approximately 2.5 and 1.5 times smaller than the one obtained with a target of Iridium. This conclusion also holds for the most accessible material presented above: Platinum.

The interplay between pair production and volume expansion is also explicitly reflected in Eq. (23). Initially, the density increases as $(L/L_r)^2$, driven by the growth of the pair multiplicity, but at a certain point, it decreases as $(L/L_r)^{-1}$ due to the expansion of the volume. By differentiating Eq. (23) with respect to the target length L/L_r , we find that the maximum of the density is reached at:

$$\frac{L_{\text{opt}}}{L_r} = \left(\frac{3}{c_2} \gamma_0 \frac{R_b}{L_r} \right)^{2/3}, \quad (25)$$

and is given by⁹:

$$\max(n_{\pm}) = c_5 n_0 \gamma_0^{4/3} \ln(\gamma_0)^2 \ln(c_1 \gamma_0) \left(\frac{R_b}{L_r} \right)^{4/3}, \quad (26)$$

where $c_5 = 3^{-2/3} c_4 c_2^{-4/3} / 2 \simeq 4.43 \times 10^{-4}$, and $n_0 = N_0/(\pi L_b R_b^2)$ is the initial electron density. Furthermore, at this optimal length, the beam radius is $R_{\pm} = 3R_b$.

Having derived the maximal density reachable, we are now in position to provide the condition for the pair plasma production as a function of the initial parameters only.

B. Conditions for pair plasma production

As we are looking for thin targets, both the incident electrons and the generated electron-positron pairs escape the material. Consequently, the outgoing beam consists of N_{\pm} positrons and $N_0 + N_{\pm}$ electrons. As a result, the quasi-neutrality, necessary for obtaining a pair plasma, can be satisfied only for the high multiplicity regime: $N_{\pm} \gg N_0$. In this regime, the pair multiplicity is accurately captured by Eq. (12). Since the target length is constrained by the radiation length, achieving this condition relies primarily on maximizing the incident electron energy.¹⁰

The second condition for achieving a pair plasma is given by comparing the skin depth (δ) to the characteristic size of the outgoing pairs (L_{\pm}). The skin depth Eq. (20) explicitly depends on the average Lorentz factor of the pairs $\langle \gamma_{\pm} \rangle$ which can be estimated as:

$$\begin{aligned} \langle \gamma_{\pm} \rangle &= \frac{\int_0^{\gamma_0} d\gamma_{\gamma} \bar{W}(\gamma_{\gamma}) w(\gamma_0, \gamma_{\gamma}) \gamma_{\gamma} / 2}{\int_0^{\gamma_0} d\gamma_{\gamma} \bar{W}(\gamma_{\gamma}) w(\gamma_0, \gamma_{\gamma})} \\ &\xrightarrow{\gamma_0 \gg 1} c_6 \gamma_0 / \ln(c_7 \gamma_0) \end{aligned} \quad (27)$$

where $c_6 = 0.359$ and $c_7 = 0.008$, and where we have considered only the first generation of pairs. In this framework, the average energy remains constant over time/target length since the cooling term in the kinetic equations [Eq. (1)] has been neglected. In simulations, the average energy exhibits a slow decay with the target length, and Eq. (27) overestimates it by at most a factor ~ 2 for $L/L_r < 1$.

Injecting Eq. (27) in Eq. (20) and considering the maximal density given by Eq. (26), we finally obtain a con-

⁷ As shown below, see also Fig. 4, the typical angular divergence of the escaping pairs is of the order of several 10s of mrad when typical LWFA beams have mrad divergence.

⁸ As the beam propagates, the longitudinal size of the beam increases due to the broad energy spectra as shown in Fig. 3 (a). Placing ourselves just after the target, we can neglect this effect.

⁹ Equations (25) and (26) are valid for $L/L_r < 1$. Typically, $R_b \sim 1 \mu\text{m}$ and $L_r \sim \ln(\gamma_0)$ mm, thus Eq. (25) holds for $\gamma_0 m c^2 \lesssim 150$ GeV.

¹⁰ At the density maximum given by Eq. (25), for $R_b \sim 1 \mu\text{m}$ and $L_r \sim \ln(\gamma_0)$ mm, Eq. (12) yields $N_{\pm} > 2N_0$ for $\gamma_0 m c^2 \gtrsim 5$ GeV

dition for collective effects¹¹:

$$r_e L_{\pm}^2 n_0 \left(\frac{R_b \ln(\gamma_0)}{L_r} \right)^{4/3} h(\gamma_0) \gg 30, \quad (28)$$

with $h(\gamma_0) = \gamma_0^{1/3} \ln(\gamma_0)^{2/3} \ln(c_1 \gamma_0) \ln(c_7 \gamma_0) \simeq 0.72 \gamma_0^{0.85}$ for $\gamma_0 \in [10^3, 10^5]$, and where the typical plasma size L_{\pm} is formally given by $\min(L_b, R_{\pm})$ but is equal to $\min(L_b, 3R_b)$ at the optimal length. For a Platinum target (optimal material for an experiment as discussed before), the previous condition can be written in the practical form, for $L_b < 3R_b$:

$$\left[\frac{\mathcal{E}_0}{10 \text{ GeV}} \right]^{0.85} \left[\frac{eN_0}{10 \text{ nC}} \right] \left[\frac{L_b}{10 \mu\text{m}} \right] \left[\frac{R_b}{5 \mu\text{m}} \right]^{-2/3} \gg 1, \quad (29)$$

and for $L_b > 3R_b$:

$$\left[\frac{\mathcal{E}_0}{10 \text{ GeV}} \right]^{0.85} \left[\frac{eN_0}{10 \text{ nC}} \right] \left[\frac{L_b}{20 \mu\text{m}} \right]^{-1} \left[\frac{R_b}{5 \mu\text{m}} \right]^{4/3} \gg 1. \quad (30)$$

These two conditions directly imply that, for a given seed electron beam charge, the best beam shape follows the proportion $L_b = 3R_b$. The condition $\delta \ll L_{\pm}$, equivalently Eqs. (28), (29) or (30), provides a clear and practical criterion for pair plasma production. These general results apply to any mono-energetic incident electron beam and can easily be extended for a source with a wide energy spectrum. However, it is important to note that the condition given in Eqs. (29) and (30) likely overestimates the onset of plasma effects.

C. Application to shower seeded by LWFA electron beam

To illustrate and validate the previous analysis, we now apply our results to a Laser Wakefield Accelerated (LWFA) electron beam colliding against a Tantalum target. The parameters of the beam are based on the LWFA beam described in [36]. It is modeled as a cylinder of charge $eN_0 = 2 \text{ nC}$, radius $R_b = 3 \mu\text{m}$, length $L_b = 10 \mu\text{m}$, and energy $\gamma_0 mc^2 = 3 \text{ GeV}$.

In Fig. 5(a), we present the pair density at the rear of the target as a function of the normalized target thickness L/L_r . Red dots are extracted from Geant4 simulations while the black line corresponds to Eq. (23). As discussed earlier, our analytical model slightly overestimates the simulated density but still shows excellent agreement in both trend and magnitude. The red and grey shaded areas represent regions where the pair multiplicity exceeds 2, respectively extracted from Geant4 simulations and Eq. (12). These regions indicate where the outgoing

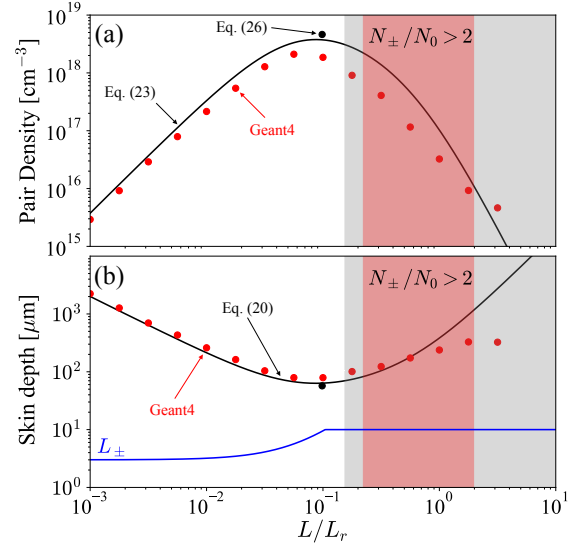


FIG. 5. In panel (a), the pair density at the rear of the target is shown as a function of target thickness L/L_r . Red points, extracted from Geant4 simulations, represent the maximum density across all space. The black line corresponds to Eq. (23), and the black dot stands for the maximum density estimated by Eqs. (26) and (25). In panel (b), the skin depth at the rear of the target as a function of the target thickness L/L_r . Red points correspond to Eq. (20) with density and average energy extracted from Geant4 simulations. The black line represents Eq. (20) calculated with Eqs. (23) and (27), while the black point is calculated using Eq. (26). The blue line indicates the typical plasma length $L_{\pm} = \min(L_b, R_{\pm})$. In both panels, the red (from Geant4) and grey (from Eq. (12)) regions correspond to $N_{\pm} > 2N_0$. Results are obtained for a cylindrical electron beam with $eN_0 = 2 \text{ nC}$, $R_b = 3 \mu\text{m}$, $L_b = 10 \mu\text{m}$, and $\gamma_0 mc^2 = 3 \text{ GeV}$ colliding with Tantalum.

bunch approaches quasi-neutrality. The boundary of the Geant4 region reflects that, for sufficiently thick targets, the produced pairs are unable to escape the material.

In panel (b), we show the corresponding skin depth as a function of the target length. The red points are extracted from Geant4 results, while the black line is calculated from Eq. (20) using Eqs. (23) and (27). As shown by the blue line representing the characteristic size of the outgoing pairs [$L_{\pm} = \min(R_{\pm}, L_b)$], the beam remains at least 10 times smaller than its skin depth for all target lengths. As a result, this typical LWFA electron beam can not produce a pair plasma when colliding with a neutral target.

This conclusion also holds for the pioneering experiment of Sarri et al. [48] in which an electron beam of energy $\gamma_0 mc^2 \sim 600 \text{ MeV}$, charge $eN_0 = 0.3 \text{ nC}$ collides with a Lead target. Considering their beam distributed in a cylinder of radius $R_b \sim 5 \mu\text{m}$ and length $L_b \sim 10 \mu\text{m}$, we obtain that the maximal density is reached for a $L \sim 5\text{-mm}$ target, in good agreement with their finding, and the number of produced pairs given by Eq. (12) aligns with their measurements. Nevertheless, the maxi-

¹¹ The numerical value is formally given by $c_6/(c_5 8\pi) \simeq 32.2$ but here we simplify it to 30

mal density given by Eq. (26) is found to be $\sim 5 \times 10^{15} \text{ cm}^{-3}$, roughly two orders below the value reported in [48]. This discrepancy arises mainly from the angular distribution of the outgoing beam, which was significantly underestimated in the original paper, as discussed in [89]. It results that the skin depth is of the order of 1 mm, ~ 100 times larger than the outgoing beam size.

This demonstrates that generating an electron-positron pair plasma by colliding an LWFA electron beam with a solid neutral target is currently unfeasible. The main limitation stems from the initial beam charge available from LWFA sources, which is well below the threshold defined by Eqs. (29) and (30) as well as by their limited dimensions. Since condition Eqs. (29) and (30) and the quasi-neutrality condition [Eq. (12) with $N_{\pm} \gg N_0$] hold for arbitrary electron source, alternative sources providing higher charge, energy or spatial dimension could be envisioned, such as electron beams from direct laser acceleration in plasma channels [22] or electron beams from solid density targets [90, 91]. In addition, while our analysis focuses on neutral targets, one could also consider employing ionized materials in which the Bremsstrahlung and Bethe-Heitler cross sections could be increased [71]. Last but not least, the approach presented in this paper can easily be generalized to consider photon-seeded sources. It is also worth noticing that the use of high-energy photon sources instead of electron beams can be an adequate solution since the quasi-neutrality is always satisfied in this geometry.

V. CONCLUSION

In conclusion, the optimal conditions for creating electron-positron plasmas from electron-seeded EMS in matter are investigated. Building on our previous work on EMS in strong-fields [68], we derive explicit expressions for the number of pairs generated from a solid target irradiated by a relativistic electron beam. These ex-

pressions, obtained considering both thin and thick targets, are in very good agreement with Geant4 simulations. The latter also provide us with a simple scaling for the angular divergence of the pairs escaping the target.

Analytical expressions are then derived for the density and characteristic size of the escaping pair jet, and a simple criterion for pair plasma production is given as a function of the driving electron beam charge, energy and characteristic size (before it enters the target). Our study thus identifies the optimal electron beam and target properties for pair plasma production in the laboratory.

We have applied our findings to the case of LWFA electron beams and demonstrated that, with current LWFA technology, the plasma state cannot be achieved. Our results are general and can be extended to other types of electron beams that may be better suited for pair plasma production. Further studies using the same methodology on ionized targets or photon sources are promising, since we believe that it could significantly increase the density of the outgoing pairs.

We believe our findings to be relevant beyond the strong-field community, to the particle physics community as they provide a predictive framework for pair production in matter for calorimetry/detector purposes, as well as to the astrophysics community, as producing pair plasmas in the laboratory could help study processes relevant to the most extreme environments in the Universe.

ACKNOWLEDGMENTS

The authors thank Sebastian Meuren, Arseny Mironov and Marija Vranic for fruitful discussions. T.G. was supported by FCT (Portugal) Grant No. CEECIND/04050/2021. Financial support by the ANR (g4QED project, Grant No. ANR-23-CE30-0011) is acknowledged.

-
- [1] H. Bethe and W. Heitler, On the stopping of fast particles and on the creation of positive electrons, *Proceedings of the Royal Society of London. Series A, Containing Papers of a Mathematical and Physical Character* **146**, 83 (1934).
 - [2] C. W. Fabjan and F. Gianotti, Calorimetry for particle physics, *Reviews of Modern Physics* **75**, 1243 (2003).
 - [3] K.-H. Kampert and A. A. Watson, Extensive air showers and ultra high-energy cosmic rays: a historical review, *The European Physical Journal H* **37**, 359 (2012).
 - [4] M. Bertolotti and M. Bertolotti, Electromagnetic showers, *Celestial Messengers: Cosmic Rays: The Story of a Scientific Adventure*, 127 (2013).
 - [5] A. Watson, The highest-energy cosmic-rays—the past, the present and the future, in *EPJ Web of Conferences*, Vol. 210 (EDP Sciences, 2019) p. 00001.
 - [6] S.-W. Bahk, P. Rousseau, T. A. Planchon, V. Chvykov, G. Kalintchenko, A. Maksimchuk, G. Mourou, and V. Yanovsky, Generation and characterization of the highest laser intensities ($10(22) \text{ w/cm}^2$), *Optics Letters* **10.1364/OL.29.002837** (2004).
 - [7] C. Hernandez-Gomez, S. Blake, O. Chekhlov, R. Clarke, A. Dunne, M. Galimberti, S. Hancock, R. Heathcote, P. Holligan, A. Lyachev, P. Matousek, I. Musgrave, D. Neely, P. Norreys, I. Ross, Y. Tang, T. Winstone, B. Wyborn, and J. Collier, The vulcan 10 pw project **10.1088/1742-6596/244/3/032006** (2010).
 - [8] D. Papadopoulos, J. Zou, C. L. Blanc, G. Chériaux, P. Georges, F. Druon, G. Mennerat, P. Ramirez, L. Martin, A. Fréneaux, A. Beluze, N. Lebas, P. Monot, F. Mathieu, and P. Audebert, The apollon 10 pw laser: experimental and theoretical investigation of the temporal characteristics, *High Power Laser Science and Engi-*

- neering 10.1017/HPL.2016.34 (2016).
- [9] *Extreme light infrastructure (ELI)*, <https://eli-laser.eu>.
 - [10] *Zettawatt-equivalent ultrashort pulse laser system (ZEUS)*, <https://zeus.engin.umich.edu>.
 - [11] C. H. Nam, J. H. Sung, H. W. Lee, J. W. Youn, and S. K. Lee, Performance of the 20 fs, 4 pw ti: sapphire laser at corels, in *CLEO: Science and Innovations* (Optica Publishing Group, 2018) pp. STu4O–3.
 - [12] C. Danson, C. Haefner, J. Bromage, T. Butcher, J. Chanteloup, E. Chowdhury, A. Galvanauskas, L. Gizzi, J. Hein, D. Hillier, N. Hopps, Y. Kato, E. Khazanov, R. Kodama, G. Korn, R. Li, Y. Li, J. Limpert, J. Ma, C. Nam, D. Neely, D. Papadopoulos, R. Penman, L. Qian, J. Rocca, A. Shaykin, C. Siders, C. Spindloe, S. Szatmári, R. Trines, J. Zhu, P. Zhu, and J. Zuegel, Petawatt and exawatt class lasers worldwide, *High Power Laser Science and Engineering* 10.1017/HPL.2019.36 (2019).
 - [13] J. Bromage, S. Bahk, I. Begishev, C. Dorrer, M. Guardalben, B. Hoffman, J. Oliver, R. Roides, E. Schiesser, M. J. S. Iii, M. Spilatro, B. Webb, D. Weiner, and J. Zuegel, Technology development for ultraintense all-opcpa systems, *High Power Laser Science and Engineering* 10.1017/HPL.2018.64 (2019).
 - [14] E. Khazanov, A. Shaykin, I. Kostyukov, V. Ginzburg, I. Mukhin, I. Yakovlev, A. Soloviev, I. Kuznetsov, S. Mironov, A. Korzhimanov, et al., exawatt center for extreme light studies, *High Power Laser Science and Engineering* 11, e78 (2023).
 - [15] A. Arefiev, V. Khudik, A. Robinson, G. Shvets, L. Willingale, and M. Schollmeier, Beyond the ponderomotive limit: Direct laser acceleration of relativistic electrons in sub-critical plasmas, *Physics of Plasmas* 23 (2016).
 - [16] H. T. Kim, V. Pathak, K. Hong Pae, A. Lifschitz, F. Sylla, J. H. Shin, C. Hojbota, S. K. Lee, J. H. Sung, H. W. Lee, et al., Stable multi-gev electron accelerator driven by waveform-controlled pw laser pulses, *Scientific reports* 7, 10203 (2017).
 - [17] A. Gonsalves, K. Nakamura, J. Daniels, C. Benedetti, C. Pieronek, T. De Raadt, S. Steinke, J. Bin, S. Bulanov, J. Van Tilborg, et al., Petawatt laser guiding and electron beam acceleration to 8 gev in a laser-heated capillary discharge waveguide, *Physical review letters* 122, 084801 (2019).
 - [18] M. Jirka, M. Vranic, T. Grismayer, and L. Silva, Scaling laws for direct laser acceleration in a radiation-reaction dominated regime, *New Journal of Physics* 22, 083058 (2020).
 - [19] H. T. Kim, V. B. Pathak, C. I. Hojbota, M. Mirzaie, K. H. Pae, C. M. Kim, J. W. Yoon, J. H. Sung, and S. K. Lee, Multi-gev laser wakefield electron acceleration with pw lasers, *Applied Sciences* 11, 5831 (2021).
 - [20] B. Miao, J. Shrock, L. Feder, R. Hollinger, J. Morrison, R. Nedbailo, A. Picksley, H. Song, S. Wang, J. Rocca, et al., Multi-gev electron bunches from an all-optical laser wakefield accelerator, *Physical Review X* 12, 031038 (2022).
 - [21] K. Poder, J. Wood, N. Lopes, J. Cole, S. Alatabi, M. Backhouse, P. Foster, A. Hughes, C. Kamperidis, O. Kononenko, et al., Multi-gev electron acceleration in wakefields strongly driven by oversized laser spots, *Physical review letters* 132, 195001 (2024).
 - [22] R. Babjak, L. Willingale, A. Arefiev, and M. Vranic, Direct laser acceleration in underdense plasmas with multi-pw lasers: a path to high-charge, gev-class electron bunches, *Physical Review Letters* 132, 125001 (2024).
 - [23] G. Sarri, D. J. Corvan, W. Schumaker, J. M. Cole, A. Di Piazza, H. Ahmed, C. Harvey, C. H. Keitel, K. Krushelnick, S. P. D. Mangles, Z. Najmudin, D. Symes, A. G. R. Thomas, M. Yeung, Z. Zhao, and M. Zepf, Ultrahigh brilliance multi-mev γ -ray beams from nonlinear relativistic thomson scattering, *Physical Review Letters* 113, 224801 (2014).
 - [24] F. Albert and A. G. Thomas, Applications of laser wake-field accelerator-based light sources, *Plasma Physics and Controlled Fusion* 58, 103001 (2016).
 - [25] Z. Gong, R. Hu, H. Lu, J. Yu, D. Wang, E.-G. Fu, J. Liu, and X. Yan, Brilliant gev gamma-ray flash from inverse compton scattering in the qed regime, *Plasma Physics and Controlled Fusion* 60, 044004 (2018).
 - [26] Y.-J. Gu, O. Klimo, S. V. Bulanov, and S. Weber, Brilliant gamma-ray beam and electron-positron pair production by enhanced attosecond pulses, *Communications Physics* 1, 93 (2018).
 - [27] C. M. Kim, C. M. Ryu, C. Zuo, and C. H. Nam, Highly efficient laser-driven compton gamma-ray source, *New Journal of Physics* 21, 033008 (2019).
 - [28] A. Formenti, M. Galbiati, and M. Passoni, Modeling and simulations of ultra-intense laser-driven bremsstrahlung with double-layer targets, *Plasma Physics and Controlled Fusion* 64, 044009 (2022).
 - [29] M. Galbiati, A. Formenti, M. Grech, and M. Passoni, Numerical investigation of non-linear inverse compton scattering in double-layer targets, *Frontiers in Physics* 11, 10.3389/fphy.2023.1117543 (2023).
 - [30] A. Matheron, J.-R. Marquès, V. Lelasseux, Y. Shou, I. A. Andriyash, V. L. J. Phung, Y. Ayoul, A. Beluze, I. Dăncuș, F. Dorchies, F. D'Souza, M. Dumergue, M. Frotin, J. Gautier, F. Gobert, M. Gugiu, S. Krishnamurthy, I. Kargaplov, E. Kroupp, L. Lancia, A. Lazăr, A. Leblanc, M. Lo, D. Mataja, F. Mathieu, D. Papadopoulos, P. San Miguel Claveria, K. Ta Phuoc, A.-M. Talposi, S. Tata, C. A. Ur, D. Ursescu, L. Văsescu, D. Doria, V. Malka, P. Ghenuche, and S. Corde, Compton photons at the gev scale from self-aligned collisions with a plasma mirror, *arXiv preprint arXiv:2412.19337* (2024).
 - [31] M. Galbiati, K. Ambrogioni, L. F. C. Monaco, M. S. G. De Magistris, D. Orecchia, F. Mirani, A. Maffini, and M. Passoni, Numerical proof-of-concept of a photon, proton, and positron laser-driven source with nanostructured targets, *arXiv preprint arXiv:2503.21630* (2025).
 - [32] H. R. Reiss, Production of electron pairs from a zero-mass state, *Physical Review Letters* 26, 1072 (1971).
 - [33] J. Shearer, J. Garrison, J. Wong, and J. Swain, Pair production by relativistic electrons from an intense laser focus, *Physical Review A* 8, 1582 (1973).
 - [34] D. Burke, R. Field, G. Horton-Smith, J. Spencer, D. Walz, S. Berridge, W. Bugg, K. Shmakov, A. Weidemann, C. Bula, et al., Positron production in multi-photon light-by-light scattering, *Physical Review Letters* 79, 1626 (1997).
 - [35] T. Blackburn, A. Ilderton, C. Murphy, and M. Marklund, Scaling laws for positron production in laser-electron-beam collisions, *Physical Review A* 96, 022128 (2017).

- [36] M. Lobet, X. Davoine, E. d'Humières, and L. Gremillet, Generation of high-energy electron-positron pairs in the collision of a laser-accelerated electron beam with a multipetawatt laser, *Physical Review Accelerators and Beams* **20**, 043401 (2017).
- [37] A. Mercuri-Baron, M. Grech, F. Niel, A. Grassi, M. Lobet, A. Di Piazza, and C. Riconda, Impact of the laser spatio-temporal shape on breit-wheeler pair production, *New Journal of Physics* **23**, 085006 (2021).
- [38] F. Salgado, K. Grafenstein, A. Golub, A. Döpp, A. Eckey, D. Hollatz, C. Müller, A. Seidel, D. Seipt, S. Karsch, et al., Towards pair production in the non-perturbative regime, *New Journal of Physics* **23**, 105002 (2021).
- [39] A. Golub, S. Villalba-Chávez, and C. Müller, Non-linear breit-wheeler pair production in collisions of bremsstrahlung γ quanta and a tightly focused laser pulse, *Physical Review D* **105**, 116016 (2022).
- [40] M. Pouyez, A. Mironov, T. Grismayer, A. Mercuri-Baron, F. Perez, M. Vranic, C. Riconda, and M. Grech, Multiplicity of electron-and photon-seeded electromagnetic showers at multipetawatt laser facilities, *Physical Review E* **110**, 065208 (2024).
- [41] K. Qu and N. J. Fisch, Creating and detecting observable qed plasmas through beam-driven cascade, *Physics of Plasmas* **31** (2024).
- [42] I. Elsner, A. Golub, S. Villalba-Chávez, and C. Müller, Entering the overcritical regime of nonlinear breit-wheeler pair production in collisions of bremsstrahlung γ -rays and superintense, tightly focused laser pulses, *Physical Review D* **111**, 096012 (2025).
- [43] E. P. Liang, S. C. Wilks, and M. Tabak, Pair production by ultraintense lasers, *Physical review letters* **81**, 4887 (1998).
- [44] C. Gahn, G. D. Tsakiris, G. Pretzler, K. J. Witte, C. Delfin, C.-G. Wahlström, and D. Habs, Generating positrons with femtosecond-laser pulses, *Applied Physics Letters* **77**, 2662 (2000), https://pubs.aip.org/aip/apl/article-pdf/77/17/2662/18552952/2662_1.online.pdf.
- [45] K. Nakashima and H. Takabe, Numerical study of pair creation by ultraintense lasers, *Physics of Plasmas* **9**, 1505 (2002).
- [46] H. Chen, S. Wilks, J. D. Bonlie, E. Liang, J. Myatt, D. Price, D. D. Meyerhofer, and P. Beiersdorfer, Relativistic positron creation using ultraintense short pulse lasers., *Physical Review Letters* **101**, 101103 (2009).
- [47] J. Myatt, J. Delettrez, A. Maximov, D. Meyerhofer, R. Short, C. Stoeckl, and M. Storm, Optimizing electron-positron pair production on kilojoule-class high-intensity lasers for the purpose of pair-plasma creation, *Physical Review E—Statistical, Nonlinear, and Soft Matter Physics* **79**, 066409 (2009).
- [48] G. Sarri, K. Poder, J. Cole, W. Schumaker, A. D. Piazza, B. Reville, T. Dzelzainis, D. Doria, L. A. Gizzi, G. Grittani, S. Kar, C. H. Keitel, K. Krushelnick, S. Kuschel, S. Mangles, Z. Najmudin, N. Shukla, L. O. Silva, D. Symes, A. Thomas, M. Vargas, J. Vieira, and M. Zepf, Generation of neutral and high-density electron-positron pair plasmas in the laboratory, *Nature Communications* **10**, 1038/NCOMMS7747 (2015).
- [49] H. Chen and F. Fiuza, Perspectives on relativistic electron-positron pair plasma experiments of astrophysical relevance using high-power lasers, *Physics of Plasmas* **30**, 020601 (2023).
- [50] C. D. Arrowsmith, P. Simon, P. J. Bilbao, A. F. A. Bott, S. Burger, H. Chen, F. D. Cruz, T. Davenne, I. Efthymiopoulos, D. H. Froula, A. Goillot, J. T. Gudmundsson, D. Haberberger, J. W. D. Halliday, T. Hodge, B. T. Huffman, S. Iaquina, F. Miniati, B. Reville, S. Sarkar, A. A. Schekochihin, L. O. Silva, R. Simpson, V. Stergiou, R. M. G. M. Trines, T. Vieu, N. Charitonidis, R. Bingham, and G. Gregori, Laboratory realization of relativistic pair-plasma beams, *Nature Communications* **15**, 10.1038/s41467-024-49346-2 (2024).
- [51] M. Lobet, C. Ruyer, A. Debayle, E. d'Humières, M. Grech, M. Lemoine, and L. Gremillet, Ultrafast synchrotron-enhanced thermalization of laser-driven colliding pair plasmas, *Phys. Rev. Lett.* **115**, 215003 (2015).
- [52] D. Uzdensky, M. Begelman, A. Beloborodov, R. Blandford, S. Boldyrev, B. Cerutti, F. Fiuza, D. Gnanios, T. Grismayer, M. Kunz, N. Loureiro, M. Lyutikov, M. Medvedev, M. Petropoulou, A. Philippov, E. Quataert, A. Schekochihin, K. Schoeffler, L. Silva, L. Sironi, A. Spitkovsky, G. Werner, V. Zhdankin, J. Zrake, and E. Zweibel, *Extreme plasma astrophysics* (2019), arXiv:1903.05328 [astro-ph.HE].
- [53] M. R. Stoneking, T. S. Pedersen, P. Helander, H. Chen, U. Hergenroth, E. V. Stenson, G. Fiksel, J. von der Linden, H. Saitoh, C. M. Surko, and et al., A new frontier in laboratory physics: magnetized electron-positron plasmas, *Journal of Plasma Physics* **86**, 155860601 (2020).
- [54] E. Williams, Nature of the high energy particles of penetrating radiation and status of ionization and radiation formulae, *Physical Review* **45**, 729 (1934).
- [55] H. J. Bhabha and W. Heitler, The passage of fast electrons and the theory of cosmic showers, *Proceedings of the Royal Society of London. Series A-Mathematical and Physical Sciences* **159**, 432 (1937).
- [56] J. Carlson and J. Oppenheimer, On multiplicative showers, *Physical Review* **51**, 220 (1937).
- [57] L. D. Landau and G. Rumer, The cascade theory of electronic showers, *Proceedings of the Royal Society of London. Series A. Mathematical and Physical Sciences* **166**, 213 (1938).
- [58] H. Snyder, Transition effects of cosmic rays in the atmosphere, *Physical Review* **53**, 960 (1938).
- [59] I. Tamm and S. Belenky, On the soft component of cosmic rays at sea level, *Journal of Physics USSR* **1**, 177 (1939).
- [60] B. Rossi and K. Greisen, Cosmic-ray theory, *Reviews of Modern Physics* **13**, 240 (1941).
- [61] G. Molière and W. Heisenberg, Cosmic radiation (1946).
- [62] J. Roberg and L. Nordheim, The angular and lateral spread of cosmic-ray showers, *Physical Review* **75**, 444 (1949).
- [63] L. Eyges and S. Fernbach, Angular and radial distributions of particles in cascade showers, *Physical Review* **82**, 23 (1951).
- [64] H. Green and H. Messel, The spread of the soft component of the cosmic radiation, *Physical Review* **88**, 331 (1952).
- [65] H. Green and O. Bergmann, Core structure in soft component showers, *Physical Review* **95**, 516 (1954).
- [66] K. Greisen, Cosmic ray showers, *Progress in Cosmic Ray Physics* **3**, 1 (1956).
- [67] K. Kamata and J. Nishimura, The lateral and the angular structure functions of electron showers, *Progress of Theoretical Physics Supplement* **6**, 93 (1958).

- [68] M. Pouyez, T. Grismayer, M. Grech, and C. Riconda, Kinetic structure of strong-field qed showers in crossed electromagnetic fields, *Physical Review Letters* **134**, 135001 (2025).
- [69] H. Koch and J. Motz, Bremsstrahlung cross-section formulas and related data, *Reviews of modern physics* **31**, 920 (1959).
- [70] J. Motz, H. A. Olsen, and H. Koch, Pair production by photons, *Reviews of Modern Physics* **41**, 581 (1969).
- [71] B. Martinez, M. Lobet, R. Duclous, E. d’Humières, and L. Gremillet, High-energy radiation and pair production by coulomb processes in particle-in-cell simulations, *Physics of Plasmas* **26** (2019).
- [72] M. Pouyez, G. Nicotera, M. Galbiati, T. Grismayer, L. Lancia, C. Riconda, and M. Grech, Supplemental material, (2025).
- [73] S. M. Seltzer and M. J. Berger, Bremsstrahlung spectra from electron interactions with screened atomic nuclei and orbital electrons, *Nuclear Instruments and Methods in Physics Research Section B: Beam Interactions with Materials and Atoms* **12**, 95 (1985).
- [74] S. M. Seltzer and M. J. Berger, Bremsstrahlung energy spectra from electrons with kinetic energy 1 keV–10 GeV incident on screened nuclei and orbital electrons of neutral atoms with $Z=1-100$, *Atomic data and nuclear data tables* **35**, 345 (1986).
- [75] NIST, Photon attenuation table, <https://physics.nist.gov/cgi-bin/Xcom/xcom2?Method=Elem&Output2=Hand>.
- [76] W. Heitler, *The quantum theory of radiation*, Oxford University Press (1954).
- [77] A. Akhiezer, N. Merenkov, and A. Rekalov, On a kinetic theory of electromagnetic showers in strong magnetic fields, *Journal of Physics G: Nuclear and Particle Physics* **20**, 1499 (1994).
- [78] J. Matthews, A Heitler model of extensive air showers, *Astroparticle Physics* **22**, 387 (2005).
- [79] Y. Selivanov and A. Fedotov, Final multiplicity of a qed cascade in generalized heitler model, *Physical Review D* **110**, 096022 (2024).
- [80] J.-N. Capdevielle and F. Cohen, The relation between the lateral profile of giant extensive air showers and the age parameter, *Journal of Physics G: Nuclear and Particle Physics* **31**, 507 (2005).
- [81] W. Apel, A. Badea, K. Bekk, A. Bercuci, J. Blümer, H. Bozdog, I. Brancus, A. Chilingarian, K. Daumiller, P. Doll, et al., Comparison of measured and simulated lateral distributions for electrons and muons with cascade, *Astroparticle Physics* **24**, 467 (2006).
- [82] R. K. Dey and S. Dam, Slope of the lateral density function of extensive air showers around the knee region as an indicator of shower age, *The European Physical Journal Plus* **131**, 402 (2016).
- [83] G. Molière, Theorie der streuung schneller geladener teilchen ii mehrfach-und vielfachstreuung, *Zeitschrift für Naturforschung A* **3**, 78 (1948).
- [84] H. A. Bethe, Molière’s theory of multiple scattering, *Physical review* **89**, 1256 (1953).
- [85] W. T. Scott, The theory of small-angle multiple scattering of fast charged particles, *Reviews of modern physics* **35**, 231 (1963).
- [86] V. L. Highland, Some practical remarks on multiple scattering, *Nuclear Instruments and Methods* **129**, 497 (1975).
- [87] G. R. Lynch and O. I. Dahl, Approximations to multiple coulomb scattering, *Nuclear Instruments and Methods in Physics Research Section B: Beam Interactions with Materials and Atoms* **58**, 6 (1991).
- [88] J. Capdevielle and J. Gawin, The radial electron distribution in extensive air showers, *Journal of Physics G: Nuclear Physics* **8**, 1317 (1982).
- [89] G. Williams, H. Chen, J. Kim, S. Kerr, and H. Khater, Comment on “table-top laser-based source of femtosecond, collimated, ultrarelativistic positron beams”, *Physical Review Letters* **124**, 179501 (2020).
- [90] X. F. Shen, A. Pukhov, and B. Qiao, Monoenergetic high-energy ion source via femtosecond laser interacting with a microtape, *Phys. Rev. X* **11**, 041002 (2021).
- [91] S. Marini, M. Grech, P. S. Kleij, M. Raynaud, and C. Riconda, Electron acceleration by laser plasma wedge interaction, *Phys. Rev. Res.* **5**, 013115 (2023).